M. U. Demirci and C. T.-C. Nguyen, "Single-resonator fourth-order micromechanical disk filters," *Proceedings*, 18th Int. IEEE Micro Electro Mechanical Systems Conf., Miami, Florida, Jan. 30 - Feb. 3, 2005, pp. 207-210.

SINGLE-RESONATOR FOURTH-ORDER MICROMECHANICAL DISK FILTERS

Mustafa U. Demirci and Clark T.-C. Nguyen

Center for Wireless Integrated Micro Systems
Department of Electrical Engineering and Computer Science
University of Michigan, Ann Arbor, Michigan 48109-2122, USA

ABSTRACT

A method for realizing a fourth-order micromechanical filter response using only a single, mass-loaded, flexural-mode disk resonator has been used to demonstrate a 20.26-MHz fourth-order Butterworth filter with a tiny 0.03% bandwidth and only 2.56 dB of insertion loss. The basic design technique uses orthogonal mode-splitting and recombining to achieve a parallel-class filter that dispenses with the need for multiple resonators and coupling links in previous filters. The single-resonator disk structure has a measured temperature coefficient of frequency TC_f of -14.2ppm/°C and a third order intercept point IIP_3 of +20.6dBm, which indicates very good device linearity.

1. INTRODUCTION

The growing demand for wireless devices capable of processing voice, image, and data, all in one handheld, has spurred great interest in technologies capable of miniaturizing the multi-reconfigurable RF front-ends needed for such flexible applications. Vibrating RF MEMS technology, with its ability to realize highly selective, low-loss, on-chip micromechanical filters [1]-[4] suitable for band or channel-selecting filter banks [5], offers a very attractive approach towards miniaturized multi-band reconfigurability. To date, mechanical filters comprised of several micromechanical resonators, coupled in some fashion, either mechanically, via soft mechanical springs [1]; or electrically, using parallel-resonator architectures [3] or coupling capacitors [4]; have been demonstrated with impressive frequency characteristics. However, as the need for banks of such filters grows, a method for reducing the number of resonators (hence, the overall complexity) required would be most welcome.

Pursuant to reducing filter complexity, this paper introduces an alternative mechanical filter architecture that uses the properly spaced orthogonal resonances from a single, mass-loaded, flexural disk resonator (c.f. Fig. 1) to generate multiple resonances without the need for multiple resonators, then combines the resonances to achieve a parallel-class filter [3]. This design technique not only dispenses with the need for multiple resonators in previous filters [1]-[4], but also removes the need for coupling links or capacitors. By reducing the complexity of high-order filter structures, this single-resonator technique stands to greatly facilitate the design of multiple-filter micromechanical circuits targeted for future wireless transceiver front-ends [5]. After describing the structure and operation of the single-resonator disk filter, this paper presents equations that simplify the design procedure, then verifies them by demonstrating a fabricated filter prototype centered at 20.26 MHz.

2. FILTER STRUCTURE AND OPERATION

Again, the principle of operation of the disk filter of this

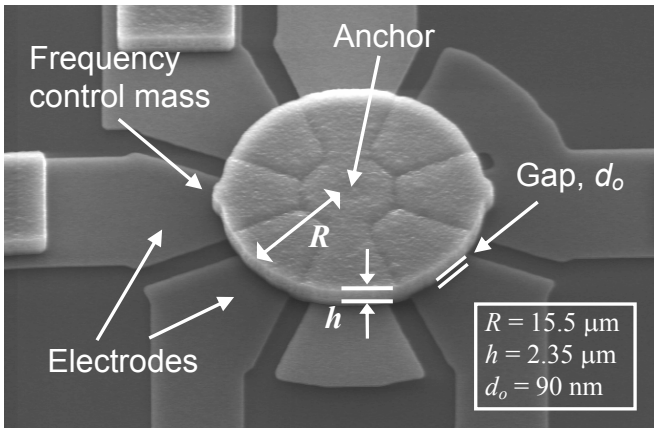

Fig. 1: SEM of a fabricated single-resonator disk filter.

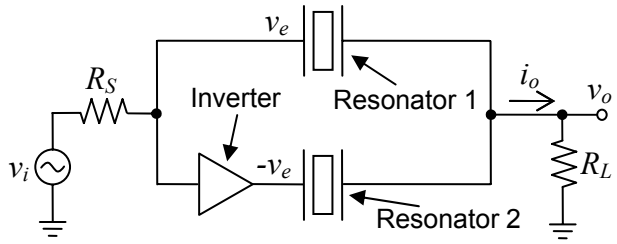

Fig. 2: Schematic of a parallel-resonator filter.

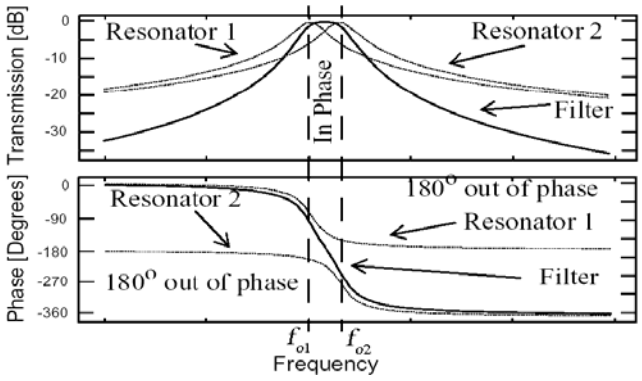

Fig. 3: Basic concept behind a parallel-resonator filter [3], where responses from two second-order resonators are added in the passband and subtracted in the stopband to achieve a fourth-order response.

work derives from the parallel filter concept [3] where the properly spaced and phased frequency characteristics of two (or more) resonators are combined to yield a flat passband and sharper roll-offs to the stopband. Fig. 2 presents circuit schematics for a filter utilizing the conventional implementation of this approach, where two resonators with frequencies f_{o1} and f_{o2} are driven by ac input voltage signals of opposite polarity, v_e and $-v_e$, and their output currents are summed by wired connections, resulting in the output spec-

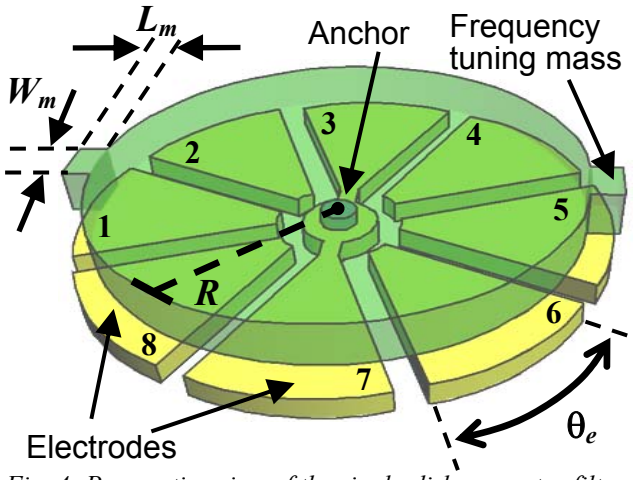

Fig. 4: Perspective view of the single-disk-resonator filter.

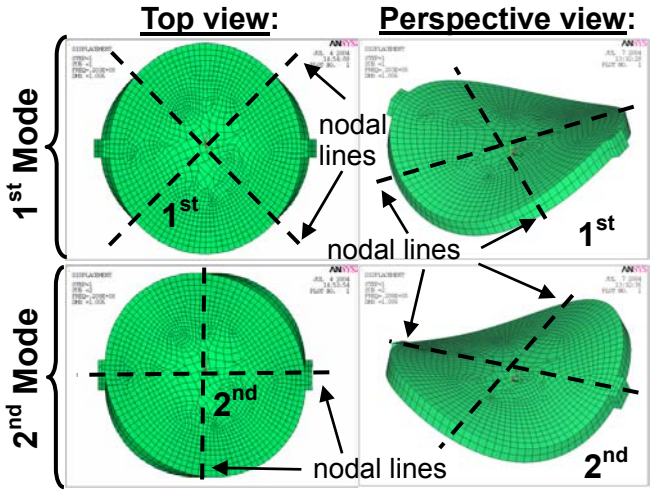

Fig. 5: ANSYS-simulated orthogonal mode shapes of the disk filter.

tra shown in Fig. 3. As seen, inputs at frequencies between the resonances of the two resonators (i.e., f_{o1} and f_{o2}) produce output currents that are in phase, and thus add, creating a passband in this frequency range that is flat when the Q's of resonators are set to the right value (to be specified later). Those at frequencies outside this interval produce output currents that are 180° out of phase, and thus subtract to provide more stopband rejection, as well as a steeper roll-off to the stopband. The bandwidth of the filter can be adjusted to a desired value by controlling the frequency separation $|f_{o1} - f_{o2}|$ and the Q of the resonators. A two-resonator filter made using this approach has fourth-order bandpass characteristics. Using a larger number of resonators, it is possible to implement higher-order filters with sharper roll-offs and larger stopband rejections.

Instead of using two resonators, however, the present filter generates two properly spaced resonances by strategically manipulating the orthogonal modes of the single, mass-loaded, flexural disk resonator presented in Fig. 4. The device consists of a polysilicon disk suspended by a centrally-located stem, over a set of eight "pie-cut" electrodes spaced 90 nm underneath, two of which are electrically connected to the center stem for dc-bias voltage access to the disk. The electrodes are identical in size to maintain symmetry in the electrostatic force distribution and in topography. As seen in the ANSYS-simulated orthogonal mode shapes in

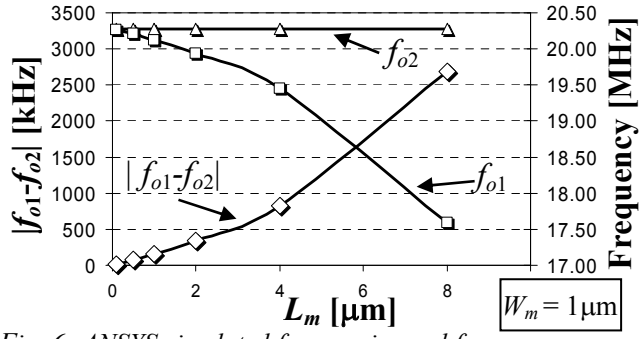

Fig. 6: ANSYS simulated frequencies and frequency separation versus length (L_m) of the frequency control masses on the perimeter of the disk structure of Fig. 4, using the disk dimensions of Fig. 1.

Fig. 5, this disk vibrates vertically over the electrodes, in a manner where adjacent quadrants move in opposite directions. The anchor at the center of the device corresponds to an effective motionless node point at which vertical energy losses to the substrate are minimized due to momentum cancellation in the bulk of the device, resulting in very high Q.

On the perimeter of the disk are two symmetrically placed masses that are essential to the operation of this filter. When located along nodal lines, such as in the 2nd mode shape schematic of Fig. 5, the masses have almost no effect on the resonance frequency; whereas at the maximum amplitude points, as in the 1st mode shape schematic of Fig. 5, they lower the frequency. By tailoring the values of the masses, a precisely controllable frequency separation between the orthogonal modes can be realized to effectively define the bandwidth of an eventual filter. Fig. 6 shows plots of frequencies f_{o1}, f_{o2} and their separation $|f_{o1} - f_{o2}|$ versus length L_m of the frequency control masses added to the perimeter of the disk (c.f. Fig. 4), obtained via ANSYS simulations using the disk dimensions of Fig. 1. As seen, frequency separations up to 2.7 MHz (i.e., 15% bandwidth) are easily achievable. The plots also show that the frequency f_{o2} of the 2nd mode is not altered by the mass addition, but rather remains equal to the resonance frequency of a disk without perimeter masses, given by [6]

$$f_{o2} = 1.556 \frac{h}{R^2} \sqrt{\frac{E}{\rho}} \qquad (1)$$

where h and R are the thickness and radius of the disk, respectively; E, ρ, and ν are the Young's modulus, density, and Poisson ratio, respectively, of its structural material.

To ensure independent access to the two modes without cross-talk, as required in a parallel-resonator filter, the electrodes underneath the disk must be placed in strategic locations. As such, electrodes 1, 3, 5, and 7 are placed under the maximum vibration amplitude regions of the 1st mode, allowing them to excite and detect this mode. These electrodes, at the same time, sit underneath the nodal lines of the 2nd mode with their center lines symmetrically aligned to the nodal lines. This positioning effectively suppresses current flow through these electrodes when the disk vibrates in the 2nd orthogonal mode of Fig. 5, since the disk moves in opposite directions at each side of the nodal line, generating equal and opposite currents that cancel into the electrode. Thus, electrodes 1, 3, 5, and 7 ideally drive and detect only

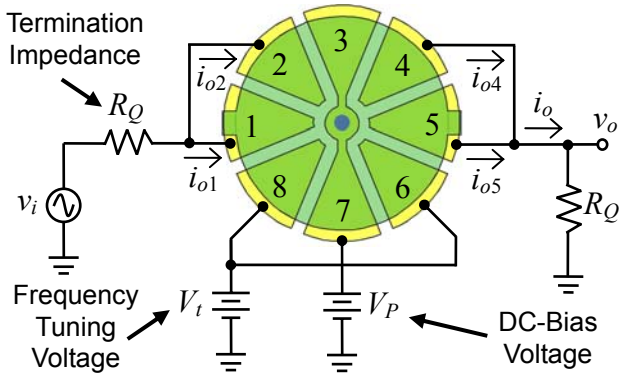

Fig. 7: Top view schematic of a single-resonator flexural-mode disk filter and its electrical bias and excitation configuration.

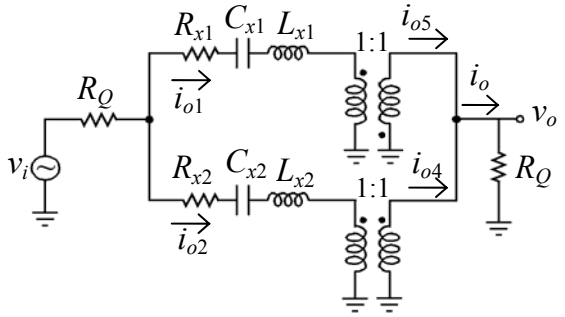

Fig. 8: Equivalent LCR circuit of the single-resonator filter of Fig. 7.

the 1st mode of Fig. 5. Similarly, electrodes 2, 4, 6 and 8 are positioned to drive and detect only the 2nd mode.

To realize the inband addition (in phase) and stopband subtraction (180° out-of-phase) depicted in Fig. 3, the excitation and detection electrodes are further configured as shown in Fig. 7. Here, the input voltage is applied (through termination resistance R_Q) to electrodes 1 and 2, which together excite both orthogonal modes with the same input phase. To detect the modes 180° out-of-phase in the stopband regions, electrodes 4 and 5 are chosen, where 5 detects the 1st mode motional current i_{o5} 180° out-of-phase with the input current i_{o1} at 1, and 4 detects the 2nd mode motional current i_{o4} in-phase with i_{o2}, where phasings are governed by the current directions indicated in Fig. 7 or Fig. 8. This phase flexibility in detection arises due to the anti-symmetry in the mode shapes; i.e., the quadrants of the 2nd mode above electrodes 2 and 4 vibrate 180° out-of-phase, whereas the quadrants of the 1st mode above 1 and 5 vibrate in phase. (Note that in-phase motion results in a negative-valued current i_{o5} going out of 5, making it 180° out-of-phase with the current i_{o1} going into 1.) Fig. 8 presents the *LCR* equivalent circuit model realized by the device configuration of Fig. 7, where the orthogonal resonances are represented by *LCR* tanks and the phase changes at the output electrodes are represented by transformers with unity turns ratios.

In addition to the above I/O terminals, electrodes 6 and 8 introduce a voltage-dependent electrical stiffness [7] that lowers the frequency of the 2nd orthogonal mode, allowing tuning of the filter passband, if needed.

3. Filter Design

Synthesis techniques for coupled resonator ladder filters are well-established, and normalized values for their transfer function coefficients are readily available from data tabulated in filter cookbooks [8]. However, such cookbooks generally tabulate data for series filters, not the parallel ones of this work. To allow the use of tabulated information for parallel-resonator filter design, a transformation is required that relates the transfer functions of series and parallel filter architectures.

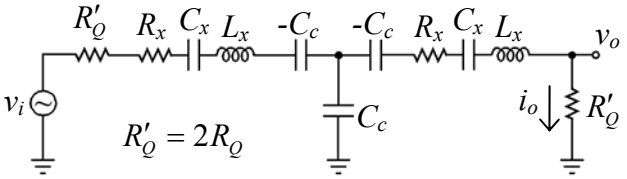

Fig. 9: Equivalent LCR circuit of a series-coupled resonator ladder filter.

Table I: Single-Resonator Disk Filter Design Data.

Parameter	Value	Parameter	Value
f_o	20.26 MHz	L_m	0.5 μm
R	15.5 μm	W_m	1 μm
h	2.35 μm	V_P	15 V
d_o	90 nm	R_x	10 kΩ
θ_e	45°	pBW	0.05%

Pursuant to attaining the needed transforming expressions, Fig. 9 presents the *LCR* equivalent circuit of a two-resonator series ladder filter, for which the lumped element transfer function is given by

$$\frac{I_o}{V_i} = \frac{-1/sC_c}{(R_x + R'_Q + sL_x + 1/sC_x)^2 - (1/sC_c)^2}. \qquad (2)$$

Note that the above assumes the typical case where the constituent resonators in the ladder are identical with frequencies equal to the filter center frequency f_o [2].

The transfer function of the parallel-resonator filter of this work is given by

$$\frac{I_o}{V_i} = \frac{(R_{x1} - R_{x2}) + s(L_{x1} - L_{x2}) + (1/sC_{x1} - 1/sC_{x2})}{(R'_Q + R_{x1} + sL_{x1} + 1/sC_{x1})(R'_Q + R_{x2} + sL_{x2} + 1/sC_{x2})}. \qquad (3)$$

For sufficiently small bandwidths (e.g., <5%), (2) and (3) are identical when frequencies f_{o1} and f_{o2} are chosen as

$$f_{o1} = f_o\left(1 - \frac{k_{12}}{Q_f}\right)^{1/2}, \quad f_{o2} = f_o\left(1 + \frac{k_{12}}{Q_f}\right)^{1/2} \qquad (4)$$

where Q_f is the filter quality factor and k_{12} is a normalized coupling coefficient between resonator tanks for a given filter type (i.e., Butterworth, Chebysev, etc) [8]. With the transformation of (4) in hand, the design of the single-resonator parallel filter with a given bandwidth (or Q_f) and center frequency reduces to the selection of proper dimensions for the disk and frequency control masses on its perimeter to attain the frequencies in (4).

The value of the Q-control resistors required to terminate this filter and the filter insertion loss are given by

$$R_Q = \frac{R_x}{2}\left[\frac{Q_{res}}{q_i Q_f} - 1\right], \quad IL = 20\log\left(\frac{2R_Q}{2R_Q + R_x}\right). \qquad (5)$$

where q_i is a normalized q parameter obtained from a filter cookbook [8].

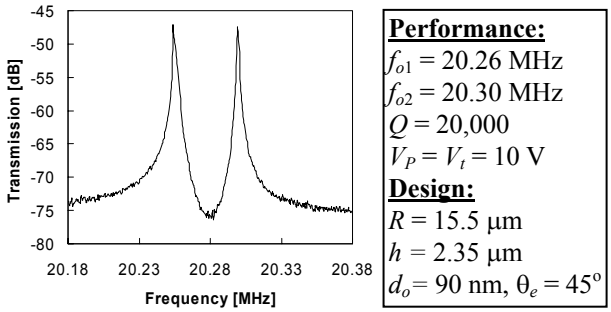

Fig. 10: Measured frequency characteristic of the two resonance modes of the disk filter of Fig. 1.

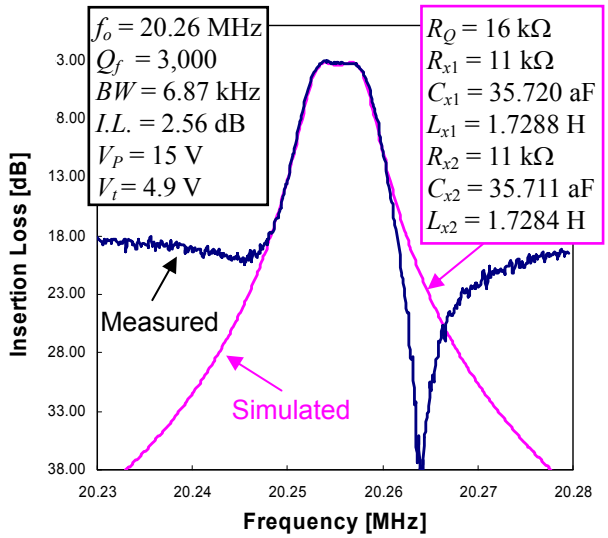

Fig. 11: Measured and simulated (via the circuit of Fig. 8) frequency characteristics for the disk filter of Fig. 1.

4. Experimental Results

2.35μm-thick, single-resonator fourth-order disk filters were designed to the specifications of Table I using the theory in Sections 2 and 3, then fabricated in a now "conventional" thin-vertical-gap surface micromachining process [2]. On-chip polysilicon termination resistors were included on the die, in series with the filters, to reduce the amount of shunt parasitic capacitance that otherwise complicates termination when off-chip resistors are used. Fig. 1 presents the SEM of a fabricated single-resonator disk filter.

Fig. 10 shows the frequency characteristics for each mode of the disk resonator of Fig. 1, measured individually under 200μTorr vacuum. The device has a Q of 20,000 at 20.26 MHz, which is quite large, clearly verifying the utility of its momentum canceling design.

Fig. 11 presents the measured frequency characteristic for the single-resonator filter of Fig. 1 hooked up as in Fig. 7, together with the theoretical curve simulated using the equivalent circuit model of Fig. 8. Here, excellent agreement is seen in the passband, verifying the theory of sections 2 and 3, However, some discrepancy is seen in the stopband, caused mainly by feedthrough distortion amplified to some degree by the high R_Q's of this realization. Nevertheless, the measured insertion loss less than 3dB is very impressive for a 0.03% bandwidth.

Fig. 12 presents a measured plot of frequency versus temperature for the disk resonator, which exhibits an extracted frequency temperature coefficient (TC_f) of -14.2 ppm/°C, which is consistent with previous polysilicon resonators [9]. Finally, to assess the linearity of the filter, Fig. 13 presents a measured plot of the output power versus two-tone (at 200 and 400 kHz offsets) and fundamental input power for the disk, from which a third order intercept point IIP_3 of +20.6dBm is observed, which indicates very good device linearity, much better than a previous clamped-clamped beam resonator [10].

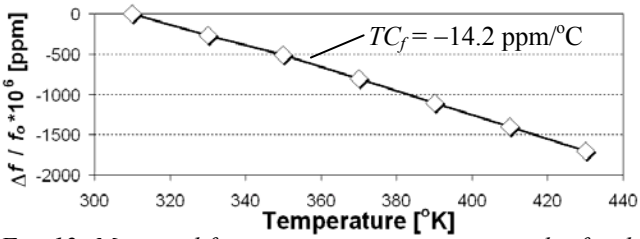

Fig. 12: Measured frequency versus temperature plot for the disk filter of Fig. 1.

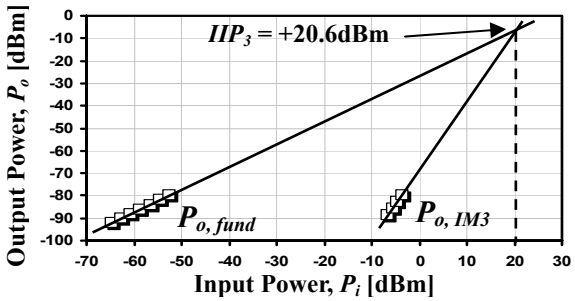

Fig. 13: Measured plot of P_o vs. P_{in} for the disk of Fig. 1, showing an extrapolated IIP_3 = +20.6 dBm.

5. Conclusions

Single-resonator, fourth-order, micromechanical disk bandpass filters based on a parallel-resonator architecture that uses orthogonal mode-splitting and recombining via a special electrode configuration has been demonstrated in a polysilicon surface-micromachining technology. Due to the high Q of the flexural disk resonator and the simple, mass-loading-based bandwidth setting technique, a tiny 0.03% bandwidth was easily achieved with an insertion loss of only 2.5dB. Bandwidths this small will likely be needed in future multi-band reconfigurable wireless transceivers, and the results demonstrated in this paper identify MEMS technology as an excellent candidate for such applications.

Acknowledgment. This work was supported by DARPA.

References

[1] K. Wang, *et al.*, *JMEMS*, 8(4), pp. 534-557, 1999.
[2] F. D. Bannon III, *et al.*, *JSSC*, vol. 35, no. 4, pp.512-526.
[3] J. R. Clark, *et al.*, "Parallel-resonator HF micromechanical bandpass filters," *Transducers'97*, pp. 1161-1164.
[4] S. Pourkamali, *et al.*, "A 600 kHz electrically-coupled MEMS bandpass filter," *MEMS'03*, pp. 702-705.
[5] C. T.-C. Nguyen, "Vibrating RF MEMS for next generation wireless applications (invited)," 2004 IEEE Custom Int. Circ. Conf., pp. 257-264.
[6] S. Timoshenko, *Vibration Problems in Engineering*, 1974.
[7] H. Nathanson, *et. al.*, *IEEE Trans. Electron Devices,* vol. ED-14, No. 3, pp. 117-133, 1967.
[8] A. I. Zverev, Handbook of Filter Synthesis, 1967.
[9] K. Wang, *et al.*, *JMEMS*, 8(4), pp. 534-557.
[10] R. Navid, *et. al.*, *Tech. Digest*, MEMS'2001, pp. 228-231.